Evaluation of the photo-catalytic degradation of pyrene using Fe-doped TiO$_2$ in presence of UV

Morteza Khodadadi Saloot[a,*], Seyed Mehdi Borghei[b], Reza Haji Seyed Mohammad Shirazi[c]

[a]*Department of Environmental Engineering, Faculty of Natural Resources and Environment, Science and Research Branch, Islamic Azad University, Tehran, Iran, email: morteza.khodadadi.s@srbiau.ac.ir*
[b]*Department of Chemical and Petroleum Engineering, Sharif University of Technology, Tehran, Iran, email: mborghei@sharif.edu*
[c]*Water and Wastewater Engineering Division, Natural Resources and Environmental Engineering Department, Tehran Science and Research Branch, Islamic Azad University, Tehran, Iran, email: r-shirazi@srbiau.ac.ir*

ABSTRACT

The oil-based compounds are widely used in modern human life, and the accidental release or leakage of these compounds is led to water and soil pollution and creates many problems for the environment. The purpose of this study was to determine the efficiency of photo-catalytic degradation of pyrene using Fe-doped TiO$_2$ in the presence of UV. This experimental study was carried out at laboratory scale in a 2 L pilot reactor. The nanoparticle was synthesized by the sol-gel method. Pyrene degradation was investigated under different conditions of pH, reaction time, nanoparticle concentration and pollutant concentration. For the statistical analysis, SPSS V.16 software and one-way analysis of variance were used. The results showed that the optimum values of studied variables were as follows: pH = 9, contact time = 45 min, initial concentration of pyrene = 25 mg/L and nanoparticle dosage = 150 mg/L. It was also observed that the highest pyrene degradation efficiency was 98.66%. The obtained results suggested that the photo-catalytic process using the doped nanoparticle revealed the excessive potential to remove and to mineralize the oil-based pollutants, and it can be considered an effective alternative for this purpose.

Keywords: Photocatalytic; Titanium dioxide; Doping; Pyrene

1. Introduction

Nowadays, the preservation of water resources, which is one of the essential human needs, has gained more importance worldwide. The population growth, the development of urbanization and industries, the rise and promotion of living standards, and the consequent need for the extraction of new resources and the introduction of new compounds into the life cycle of human beings have led to the contamination and limitation of the existing water resources, and has caused the water crisis for a near future. Currently, the situation is such that the disposal of waste and wastewater cannot be a successful approach, but the only acceptable approach is the proper treatment of wastewater and its reuse. The importance of this issue becomes more apparent when it is taken into consideration that Iran has located in desert and semi-desert region. In recent years, the climate change and the phenomenon of global warming have deteriorated the situation of the region, and the continuation of this process will force us to deliberately change our approach, especially on the issue of wastewater reuse [1–4].

A large number of synthetic organic chemical pollutants and, sometimes emerging pollutants, are daily released through the wastewaters into the environment and water resources. As mentioned above, in our country, they are also produced by various sources, including agricultural and

* Corresponding author.

industrial activities such as oil and petrochemical industries, oil refineries, chemical manufacturing industries, paper manufacturing, food industry, etc. Some of these pollutants are non-degradable or toxic to the biological system and are considered as a deterrent. In natural environments, these compounds have a long lifespan and are slowly decomposed. The aromatic and cyclic organics are of these compounds [1,2]. The polycyclic aromatic hydrocarbons (PAHs) are carcinogenic and mutagenic compounds [5,6]. These compounds are often found in form of complex compounds in the environment and are rarely seen in a single state. These compounds are usually colorless to white or pale yellow and they are used in the painting, plastics, pesticides and asphalt [7]. Pyrene is one of the compounds of this group, which contains four benzene rings (Fig. 1). Its chemical formula is $C_{16}H_{10}$ and its molecular weight is 202.26 g/mol. The density and boiling point of this compound are 1.27 g/cm^3 and 404°C, respectively and its solubility in water is 0.135 mg/L. Pyrene and its derivatives are commercially used in paint, insecticides, pharmaceuticals and plastics industries. Pyrene is a symmetric hydrocarbon containing four aromatics linked together and is introduced as one of the priority pollutants by the US Environmental Protection Agency (USEPA) [5,8,9].

Sometimes, the use of conventional treatment techniques is not effective in removing these compounds to meet the standard levels. In recent years, the advanced oxidation processes (AOPs) have been developed to obtain advanced wastewater treatment [10,11]. AOPs produce strong oxidation agents (hydroxyl radicals) that are able to complete decomposition of wastewater contaminants [12]. One of the most important wastewater treatment technologies is the photo-catalytic and semiconductor process, which has been shown to be beneficial for treating wastewater pollutants [13,14]. Among the various semiconductor materials (oxides, sulfides, etc.), TiO_2 has become more appealing due to high photocatalytic activity, steady chemical resistance to light corrosion, economic acceptability, low cost, and lack of toxicity [15,16]. The semiconductors with small band gap energy show a better absorption spectrum in the sun. Thus, for better utilization of sunlight, a small band gap semiconductor is the better choice. Selecting a semiconductor photo-catalyst, depending on its application, is often affecting the balance between factors such as high oxidation power, appropriate overlapping with the sunlight spectrum, and chemical and photochemical stability. Titanium dioxide has a good chemical and photochemical stability and high
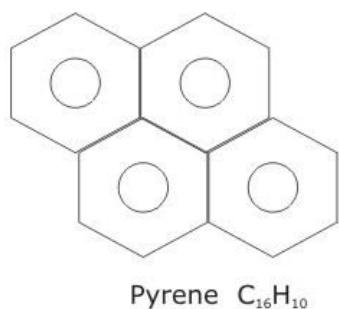
oxidation power (E = 1.3 V) among various semiconductors. But its weak overlapping with the sunlight spectrum limits these excellent properties as photo-catalyst [17,18]. Therefore, in this study, the doping was used to solve this problem, because the band gap energy is shortened by doping and the wavelength range received from the UV range is entered into the visible range [19].

In this study, the degradation efficiency of pyrene was investigated using the Fe-doped TiO_2 Nanoparticles in the presence of UV. Moreover, the effects of different parameters, that is, solution pH, catalyst dosage, initial pyrene concentration and reaction time were studied in the presence of UV irradiation. The mineralogy of Fe-doped TiO_2 nanoparticles was characterized by X-ray diffraction (XRD) techniques, and the surface morphology properties of Fe-doped TiO_2 nanoparticles were determined using the scanning electron microscope (SEM) technique. Furthermore, by-products of pyrene photodegradation were determined using a gas chromatography–mass spectroscopy (GC-MS).

2. Materials and methods

All of the chemicals used in this study were purchased from the Sigma Aldrich Co. (USA). These chemicals were of analytical grade. The Fe-doped TiO_2 was synthesized through the sol-gel method to apply as a catalyst. The double distilled water was used for preparing the solution, and the solution pH was regulated using the 1 M NaOH and HCl.

This study was an experimental-lab scale study which was conducted to evaluate the efficacy of the photo-catalytic degradation of pyrene from aqueous solution using the Fe-doped TiO_2 in the presence of UV. This study was conducted in the 2 L pilot reactor (made of Pyrex) with a diameter of 14 cm and a height of 18 cm. A medium pressure Lamp UV (30 watt, length of 6.5 cm and a diameter of 1 cm and coating quartz with an external diameter of 26 mm, an internal diameter of 23 mm and a length of 90 cm) has been established in the center of the reactor lid which was made of multilayer aluminum foil. The sampling was carried out through another hole on the reactor lid (Fig. 2).

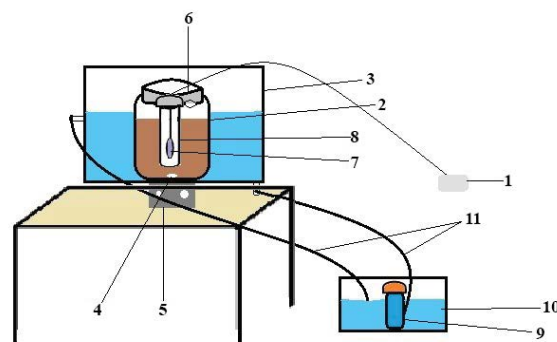Fig. 1. Chemical structure of pyrene.

Fig. 2. Schematic of the reactor used in the process. (1) trans of lamp 150 W, (2) glass reactor, (3) cooling water, (4) magnet (5) magnetic stirrer (6) reactor doors, (7) UV lamp 150 W medium pressure (8) covering quartz, (9) pump, (10) the water tank and (11) pipes for water.

The maximum wavelength of the used UV lamp was the 247.3 nm and in range of UV-C. To preserve against the UV lamp radiation, the reactor was covered by the aluminum foil. The mixing was done in the reactor using a magnetic stirrer and magnet. Inside the reactor, the 5.5 cm of free height was considered for moving the magnet. Sampling was performed at different times and the process of removal of oil compounds in this reactor was investigated. In order to remove the TiO_2 nanoparticles, the sample was centrifuged at 4,000 rpm for 30 min.

The degradation efficiency is calculated by Eq. (1):

$$Degradation\,(\%) = \left(\frac{C_0 - C_t}{C_0} \right) \times 100 \qquad (1)$$

where C_0 and C are the initial and final concentration of pyrene, respectively.

The parameters studied were included the initial concentrations of pyrene (1–100 mg/L), contact time (10–180 min), the pH values (3–11) and the nanoparticle dosage of 50–300 mg/L. The residual concentration of pyrene was also measured by the high performance liquid chromatography (HPLC). HPLC Agilent 1260 infinity (Agilent Technologies Co. Ltd., USA) equipped with a Shimadzu LC-20 AB pump: 140 mm × 260 mm × 420 mm, operating temperature range: 4°C–35°C, power requirements: 100 VAC, 150 VA, 50/60 Hz, maximum discharge pressure: 40 MPa, A C18 column (250 mm × 4.6 mm, with 5 μm particle size, pore size: 12 nm) was used as the stationary phase, and a UV-Vis spectrophotometer (Shimadzu UV-1600, Japan), dimensions: 380 mm (200 mm) × 550 mm × 470 mm, power consumption: 160 VA, frequency: 50/60 Hz, wavelength range: 190 to 1,100 nm, wavelength accuracy: ±0.5 nm, wavelength repeatability: ±0.1 nm, photometric range: absorbance: −0.5 to +3.999 Abs, photometric accuracy (at 0.5 Abs): ±0.002 Abs, photometric repeatability (at 0.5 Abs): ±0.001 Abs). The mobile phase was a mixture of acetonitrile and water (90:10 v/v, HPLC grade, Merck, Germany) with a flow rate of 1 mL/min. GC-MS (Varian-GC-MS 4000) instrument was applied for the explanation of pyrene degradation pathways. The GC column used for separation was an HP-5, (30 m × 0.25 mm) internal diameter. The film thickness was 0.25 μm. The carrier gas was helium with a flow rate of 1 mL/min. All experiments were performed triplicate.

The mineralogy of Fe-doped TiO_2 nanoparticles was also characterized by XRD techniques (Rigaku RINT2200, Japan), and the surface morphology properties of Fe-doped TiO_2 nanoparticles were determined using the SEM technique (model KYKY EM3200, Japan). The statistical analysis was performed using SPSS V.16 software and one-way analysis of variance (ANOVA).

3. Results

3.1. Properties of nanoparticles

Fig. 3 shows the SEM image and the diagram of the diameter distribution of TiO_2 nanoparticles before doping with iron. The mean diameter of particles confirmed that TiO_2 particles are nano-sized particles. The mean diameter of the nanoparticles was observed to be 42.4 nm.

Fig. 3 shows the SEM image and the diameter distribution diagram of TiO_2 nanoparticles after doping with iron. The mean diameter of the Fe-doped TiO_2 nanoparticles is 37.89 nm; the comparison of TiO_2 and Fe-TiO_2 NPs using SEM image (Figs. 3–5) showed that the structure of the Fe-doped TiO_2 nanoparticle had lower size. It is also revealed that the mean particle size of Fe-doped TiO_2 was smaller. Furthermore, it was clarified that the mean size of Fe-doped TiO_2 nanoparticles (Fig. 4) is smaller than TiO_2 nanoparticles (Fig. 6).

Fig. 7 shows the XRD pattern for Fe-doped TiO_2 nanoparticles. Considering the peaks found in the XRD pattern
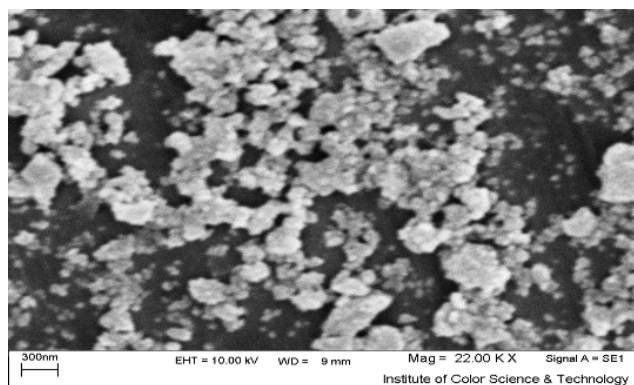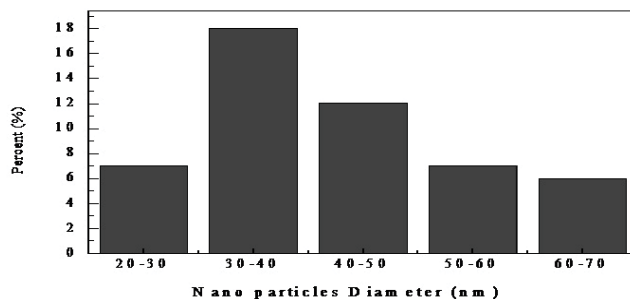
Fig. 3. SEM TiO_2 nanoparticle.
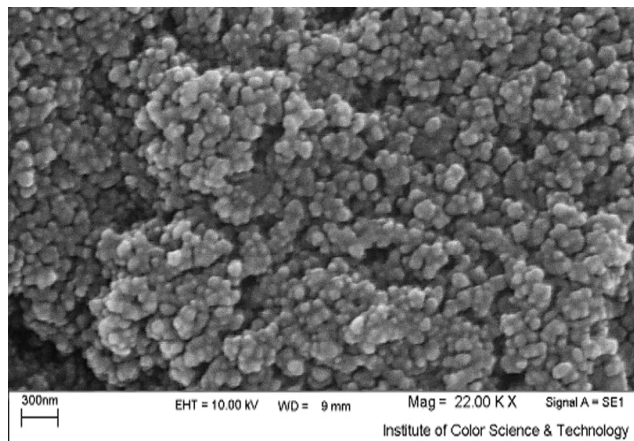
Fig. 4. TiO_2 nanoparticles diameter (nm).

Fig. 5. SEM image of a Fe-TiO_2 nanoparticle.

Fig. 6. Mean diameter of Fe-TiO$_2$ nanoparticle.

Fig. 7. X-ray diffraction pattern for Fe-doped TiO$_2$ nanoparticles.
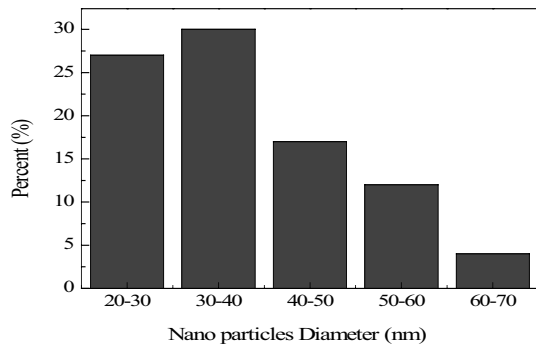
(at 25° maximum peaks), the Fe-doped TiO$_2$ consists of anatase structure.

The peaks of the rutile phase at the angles of 27°, 36°, 56°, and 64° are represented as (110), (101), (220), and (310) planes, respectively. On the other hand, the peaks at 25° and 48° show the TiO$_2$ in the Anatase phase. Fig. 7 shows that the highest amount is related to the Anatase phase while the Rutile phase heterogeneously exists with the Anatase phase. Titanium dioxide is found in three crystalline forms of Anatase, Rutile and Brucite; among them, only anatase and rutile have a light catalytic activity. The light activity is higher in Anatase phase compared to the Rutile and therefore it is more applicable.

3.2. Determination of optimum pH for degradation of the pyrene from the aqueous medium

Fig. 8 shows the optimum pH for the degradation of pyrene from the aqueous solution at different pH values. According to the results, at constant values of time (60 min), pyrene concentration (50 mg/L) and nanoparticles concentration (100 mg/L) and different values of pH (3–11), the highest degradation percentage was observed in pH values of 11 (90.76%) and 9 (89.5%). One-way ANOVA showed that the mean degradation percentage at different pH values was significantly different (P-value < 0.001). Also, by performing multiple comparison tests of least significant difference (LSD) and Duncan, it was found that the average degradation efficiency at pH of 9 and 11 was the same. Hence, the pH of 9 was selected as optimum pH in this study (P-value = 0.817).

3.3. Determination of optimum experimental period for pyrene degradation from the aquatic environment

Fig. 9 illustrates the pyrene degradation efficiency at different reaction times in the aqueous medium. Taking into account the constant concentration of pyrene (50 mg/L), the constant values of nanoparticles concentration (100 mg/L), pH of 9 and different reaction time, the highest degradation efficiency (93.66%) was achieved at 90 min. One-way ANOVA showed that there was a statistically significant difference in mean degradation efficiencies obtained at 10, 30 and 45 min (P-value < 0.001). Moreover, the Duncan (Table 1) and LSD test showed that the mean degradation efficiency at 45 and 60 min was not statistically significant (P-value = 0.62).
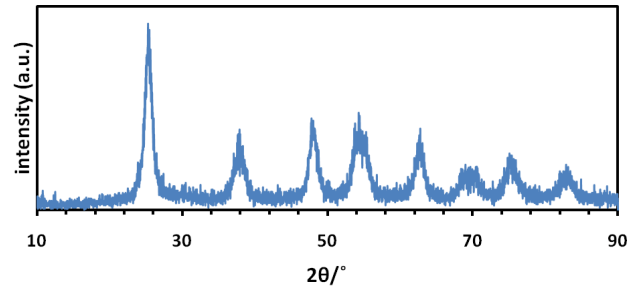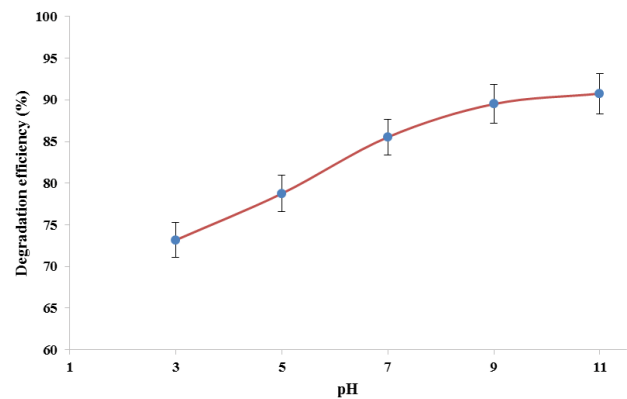

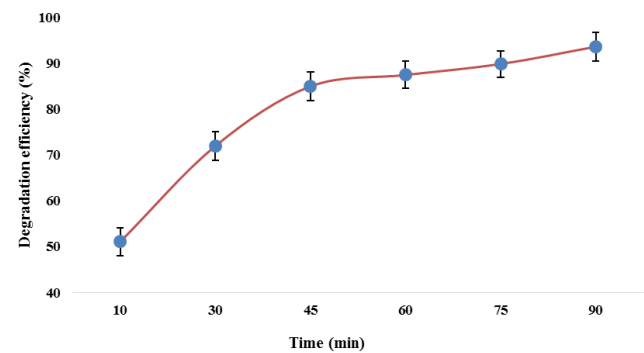Fig. 8. Optimal pH for degradation of pyrene in the aqueous solution.

Fig. 9. Optimum time for degradation of pyrene from the aquatic environment.

Base on the above results, the optimal reaction time was considered to be 45 min.

Table 1 also shows the pyrene degradation efficiency at different reaction times. As can be seen, the removal efficiency increases by increasing time. The lowest degradation efficiency (50.6%) is related to the reaction time of 10 min, and the highest degradation efficiency (93.66%) is related to 90 min.

3.4. Effect of the initial concentration of pyrene on the removal efficiency

Fig. 10 reveals the effect of the initial concentration of pyrene (5, 10, 25, 50 and 100 mg/L) on degradation efficiency

Table 1
Degradation efficiency at different times

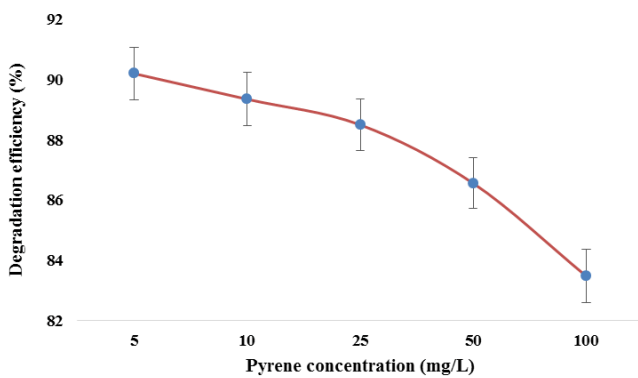| Time	Initial concentration	Secondary concentration	Degradation efficiency
10	50	24.7	50.6
30	50	12.93	74.14
45	50	6.84	86.32
60	50	5.58	88.84
75	50	4.27	91.46
90	50	3.17	93.66

Fig. 10. Variation of degradation efficiency by the pyrene concentration.

Table 2
Comparison of mean degradation efficiency at different times using Duncan test

	Time	Subset for alpha = 0.05			
		1	2	3	4
Duncan[a]	10	50.6000			
	30		74.1400		
	45			86.5100	
	60			88.8400	
	75				91.4600
	90				93.6600
	Sig.	1.000	1.000	0.062	0.076

using the constant nanoparticles concentration (100 mg/L) at the pH of 9 and reaction time of 45 min. As observed, the highest degradation efficiency (90.2%) was obtained at the initial concentration of 5 mg/L. One-way ANOVA showed that the mean degradation efficiency at different initial concentrations of pyrene was statistically significant (P-value = 0.002).

Table 3 shows the comparison of the mean degradation efficiencies achieved at different concentrations using Duncan's test. The mean degradation efficiency at the initial concentration of 100 mg/L (83.076% ± 1.803%) is different from other concentrations (P-value < 0.05). Also, the mean degradation efficiency at the initial concentration of 50 mg/L

is different from all initial concentrations except for the initial concentration of 25 mg/L (P-value = 0.138). Considering that the results of one-way ANOVA and LSD and Duncan tests showed that the mean degradation efficiencies at the initial concentration of 25 and 50 mg/L are the same (P-value = 0.138) and are different from other subsequent concentrations (0.05 > P-value); Thus, the optimum initial concentration was 25 mg/L (Table 2).

3.5. Effect of the nanoparticle concentration on the removal efficiency

Fig. 11 shows the variation of degradation efficiencies versus the changes in nanoparticle concentration. The experiments of this section were carried out using different concentrations of nanoparticles (50, 100, 150, 200, 250 and 300 mg/L) at constant values of pyrene concentration (25 mg/L), pH of 9 and reaction time of 45 min. The highest degradation efficiency (97.92%) was at the initial concentration of 300 mg/L. One-way ANOVA showed that the mean degradation efficiency at different concentrations of nanoparticles was statistically significant ($P < 0.001$).

Table 4 shows the comparison of the mean degradation efficiency at different concentrations of nanoparticles using Duncan's test. The results of one way ANOVA and LSD and Duncan tests showed that the mean degradation efficiency was same (P-value = 0.295) at the nanoparticle concentration of 150 and 200 mg/L, while it was different in other concentrations (P-value > 0.05). Therefore, the optimum nanoparticle concentration was selected as 150 mg/L.

Table 3
Comparison of the mean degradation efficiencies at different concentrations using Duncan test

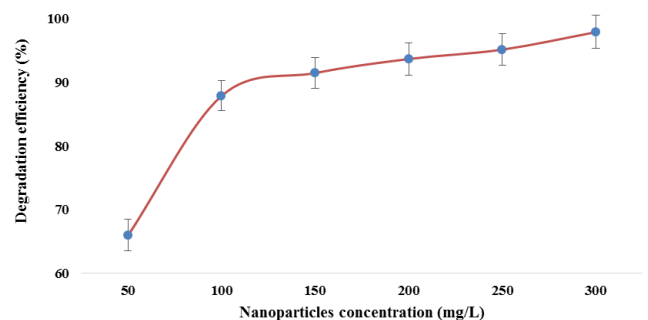| Initial concentration of pyrene	Subset for alpha = 0.05		
	1	2	3
100	83.0767		
50		86.2400	
25		88.3933	88.3933
10			89.6000
5			90.2000
Sig.	1.000	0.138	0.225

Fig. 11. Variation of degradation efficiency by the nanoparticles concentration amount.

Table 4
Comparison of the mean degradation efficiency at different concentrations of nanoparticles

Nanoparticle concentration	Subset for alpha = 0.05			
	1	2	3	4
50	65.5600			
100		89.1733		
150			91.5600	
200			92.6400	
250				95.3600
300				97.2800
Sig.	1.000	1.000	0.295	0.076

3.6. Comparison of the pyrene degradation using pure TiO₂ and Fe-doped TiO₂

Fig. 12 shows the results related to the degradation of pyrene by pure TiO_2 and Fe doped TiO_2 in optimal condition. Considering this figure, pyrene degradation efficiency by Fe-TiO_2 NPs was much higher compared to pure TiO_2; so that the highest degradation efficiency by pure TiO_2 and Fe-TiO_2 NPs, at 60 min, was achieved to be 47.52% and 98.93%, respectively.

3.7. Identification of by product in the photocatalytic degradation of pyrene

To determine intermediates and by products in the photocatalytic degradation of pyrene using Fe-doped TiO_2 in the presence of UV, a series of experiments were carried by GC-MS out at optimum conditions (pH = 9, reaction time = 45 min, pyrene concentration = 25 mg/L, nanoparticle concentration = 150 mg/L). The identified products and pyrene degradation pathways by GC-MS have been shown in Table 5. The main products were pyrene, 1,6-pyrene quinone + 1,8-pyrene quinone, monohydroxypyrene, 4-(1-hydroxynaphthalen-2-yl)-2-oxo-but-3-enoic acid, 2-hydroxybenzalpyruvic acid, salicylic acid, 9,10-phenanthrenequinone, dibutyl phthalate and 1-methoxyl-2-H-benzo[h]chromene-2-carboxylic acid.

4. Discussion

As it is known, the pH is considered as the most effective parameters that can influence the surface charge properties of the photocatalyst. Furthermore, the production of the oxidizing agents, e.g., OH• radicals are controlled by this parameter [20]. As it was observed, the optimum pH for eliminating the pyrene in this study was obtained to be 9; so that, the higher degradation efficiency was achieved at this pH using lower UV/Fe-doped TiO_2 doses. It has reported that the photocatalyst activity seriously depends on the amount of adsorbed pollutant over photocatalyst and it means that the reason for increasing the photocatalytic degradation of the pyrene may be due to its higher adsorption on the surface of nanoparticle [21]. Moghaddam et al. [22] study showed that increasing pH value is led to

an increase in OH radicals in the solution and this increase is led to higher degradation efficiency of phenol. Felix et al. [23] have conducted a photocatalytic degradation process to eliminate the Naphthalene, and they observed that the highest removal efficiency is achieved to be 92% at the pH of 9 which it agreed with the results of the present study. Abdollahi et al. [24] studied the photo-catalytic degradation efficiency m-cresol by zinc oxide under visible-light Irradiation, and they observed that the best results are achievable at pH of 9, which is in accordance with the results of this study.

The results of the present study revealed that the reaction time is one of the effective parameters on the degradation of the pyrene. It was observed that the degradation efficiency was increased by increasing the time. This is consistent with the results of various studies in this regard. It may be due to this fact that increasing the reaction time has provided enough time to produce reactive hydroxyl radicals and to react the active hydroxyl radicals with the pollutant, which is led to increasing the degradation efficiency [25]. Bazrafshan et al. [26] conducted a study to investigate the Aniline photo-catalytic degradation efficiency using the magnesium oxide nanoparticles and observed that increasing the time has a positive effect on degradation efficiency. Furthermore, Kumar and Pandey [27] have also reported in their study that increasing the reaction time had a remarkable effect and increased the degradation efficiency of the pollutants, which verifies our results.

The results also showed that the degradation efficiency was decreased by increasing the concentrations of the pollutant. Rajamanickam and Shanthi [28] have also observed that the degradation efficiency is significantly affected by the pollutant concentration; so that it was decreased by increasing the pollutant concentration. Increasing the pollutant concentration is led to greater absorption of the photons by pollutant and decreasing their absorption by the catalyst, which is resulted in the reducing the degradation efficiency; this can confirm and can describe our results [28]. This is also consistent with the studies of Borghei [29], Sahu [30] and Chun-li [31]. Zhou et al. [32] have also recognized that the TiO_2 is effective in photo-catalytic removal of pollutant, which confirms the results of the present study.
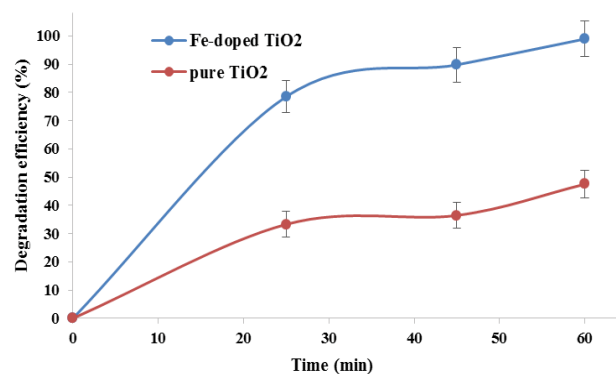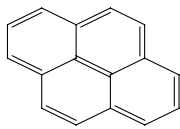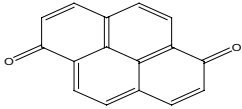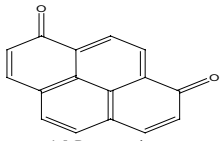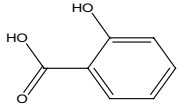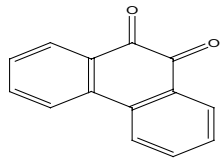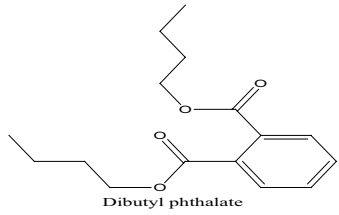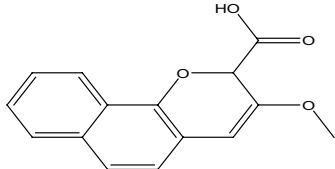
Fig. 12. Degradation efficiency for pyrene by the pure TiO_2 and Fe-doped TiO_2 (pH = 9, pyrene concentration = 10 mg/L and nanoparticle concentration = 300 mg/L).

Table 5
Pyrene degradation pathways estimated by GC-MS data

Intermediate molecular structure	Molecular weight (g/mol)	Molecular formula
pyrene	202.2	$C_{16}H_{10}$
1,6-Pyrene quinone	232	$C_{16}H_8O_2$
1,8-Pyrene quinone	232	$C_{16}H_8O_2$
Monohydroxypyrene	240	
4- (1-hydroxynaphthalen-2-yl)-2- oxo-but-3-enoic acid	242	$C_{14}H_{10}O_4$
2-hydroxybenzalpyruvic acid	192	$C_{10}H_8O_4$
Salicylic acid	138	$C_7H_6O_3$
9,10-Phenanthrenequinone	208	$C_{14}H_8O_2$
Dibutyl phthalate	278	$C_{16}H_{22}O_4$
1-methoxyl-2-H-benzo[h]chromene-2-carboxylic acid	302	$C_{16}H_{14}O_6$
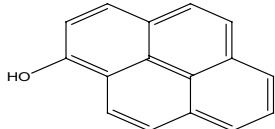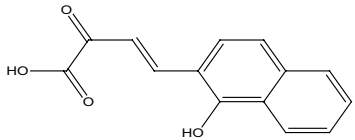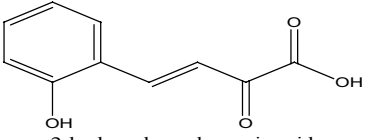
The result of this study showed that the optimum concentration of nanoparticles is 150 mg/L. Therefore, according to the results of this study, the highest degradation efficiency was observed in the presence of very low concentrations of nanoparticles; the main reason for this event can be due to the doping the nanoparticles of titanium dioxide. Zazouli et al. [33] conducted a study to degrade the furfural using the TiO_2/SUN and TiO_2/UV processes and identified that the degradation efficiency is obtained at a lower concentration of nanoparticles. The efficiency of the TiO_2/SUN process was insignificant compared to TiO_2/UV process which its reason is the TiO_2 band gap absorbing beams with a wavelength of 278 nm and lack of ability to absorb the wide range of solar beams. The doped nanoparticles are able to absorb a wider range of solar wavelengths due to shortening the band gap; thus, they have higher degradation efficiency, which confirms our results [33].

To explain the effect of nanoparticle concentration and increasing the degradation efficiency by increasing the photo-catalyst, it can be said that increasing the catalyst concentration increases the number of absorbed photons and an increase in photo-catalyst concentration up to optimum levels can increase the photo-catalytic degradation. Similar results were also observed in the study conducted by Rajamanickam and Shanthi [28], these researchers identified that the degradation efficiency is increased by increasing the catalyst concentration up to the optimum amount and reported that it is due to increasing the absorption of photons and adsorption of pollutant molecules by increasing the photo-catalyst [28].

5. Conclusion

This study was carried to estimate the efficiency of the photo-catalytic process (Fe-doped TiO_2 in the presence of UV) in the degradation of pyrene. The results showed that the studied system has great efficiency in the degradation of pyrene. Moreover, it was observed that decreasing initial concentration of pyrene and increasing reaction time, pH solution and nanoparticles concentration have lied to accelerate the degradation of pyrene. Furthermore, in this study, the optimum laboratory conditions for degradation of pyrene were as follows: pH solution of 9, reaction time of 45 min, initial pyrene concentration of 25 mg/L and nanoparticles concentration of 150 mg/L. The highest pyrene degradation efficiency was obtained to be 98.66%. Moreover, according to the results obtained, the pyrene degradation efficiency using Fe-doped TiO_2 nanoparticles was much higher compared to the pure TiO_2. Based on the results, it can be concluded that photo-catalytic process (Fe-TiO_2 NPs in the presence of UV) has an acceptable efficiency in degradation pyrene and could be used as an appropriate pretreatment in treating wastewaters containing oil compounds such as pyrene.

References

[1] R. Shokoohi, A.J. Jafari, A. Dargahi, Z. Torkshavand, Study of the efficiency of bio-filter and activated sludge (BF/AS) combined process in phenol removal from aqueous solution: determination of removing model according to response surface methodology (RSM), Desal. Wat. Treat, 77 (2017) 256–263.

[2] A. Dargahi, M. Mohammadi, F. Amirian, A. Karami, A. Almasi, Phenol removal from oil refinery wastewater using anaerobic stabilization pond modeling and process optimization using response surface methodology (RSM), Desal. Wat. Treat, 87 (2017) 199–208.

[3] D. Balarak, Y. Mahdavi, Experimental and kinetic studies on acid red 88 dye (AR88) adsorption by Azolla filiculoides, Biochem. Physiol., 5 (2016) 2.

[4] R. Shokoohi, R. Azami Gillani, M. Molla Mahmoudi, A Dargahi, Investigation of the efficiency of heterogeneous Fenton-like process using modified magnetic nanoparticles with sodium alginate in removing Bisphenol A from aquatic environments: kinetic studies, Desal. Wat. Treat, 101 (2018) 185–192.

[5] R. Shokoohi, H. Movahedian, A. Dargahi, A.J. Jafari, A. Parvaresh, Survey on efficiency of BF/AS integrated biological system in phenol removal of wastewater, Desal. Wat. Treat., 82 (2017) 315–321.

[6] G. Coral, S. Karagoz, Isolation and characterization of phenanthrene-degrading bacteria from a petroleum refinery soil, Soil Microbiol., 55 (2005) 255–259.

[7] D. Boyle, C. Wiesner, A. Richardson, Factors affecting the degradation of polyaromatic hydrocarbons in soil by white-rot fungi, Soil Biol. Biochem., 30 (1998) 873–882.

[8] C. Kazunga, M.D. Aitken, Products from the incomplete metabolism of pyrene by polycyclic aromatic hydrocarbon-degrading bacteria, Appl. Environ. Microbiol., 66 (2000) 1917–1922.

[9] Y. Hu, F. Ren, P. Zhou, M. Xia, S.J. Liu, Degradation of pyrene and characterization of *Saccharothrix* sp. PYX-6 from the oligotrophic Tianchi Lake in Xinjiang Uygur Autonomous Region, China, Chin. Sci. Bull., 48 (2003) 2210–2215.

[10] A. Dargahi, D. Nematollahi, G. Asgari, R. Shokoohi, A. Ansari, M.R. Samarghandi, Electrodegradation of 2, 4-dichlorophenoxyacetic acid herbicide from aqueous solution using three-dimensional electrode reactor with G/β-PbO₂ anode: Taguchi optimization and degradation mechanism determination, RSC Adv., 8 (2018) 39256–39268.

[11] A. Zarei, H. Biglari, M. Mobini, A. Dargahi, G. Ebrahimzadeh, M.R. Narooie, Disinfecting poultry slaughterhouse wastewater using copper electrodes in the electrocoagulation process, Pol. J. Environ. Stud., 27 (2018) 1907–1912.

[12] A.M. Amat, A. Arques, F. López, M.A. Miranda, Solar photocatalysis to remove paper mill wastewater pollutants, Solar Energy, 79 (2005) 393–401.

[13] S.K. Kansal, M. Singh, D. Sud, Studies on photodegradation of two commercial dyes in aqueous phase using different photocatalysts, J. Hazard. Mater., 141 (2007) 581–590.

[14] M. Uğurlu, M.H. Karaoğlu, Removal of AOX, total nitrogen and chlorinated lignin from bleached Kraft mill effluents by UV oxidation in the presence of hydrogen peroxide utilizing TiO_2 as photocatalyst, Environ. Sci. Pollut. Res., 16 (2009) 265–273.

[15] N. Guettaï, H. Ait Amar, Photocatalytic oxidation of methyl orange in presence of titanium dioxide in aqueous suspension. Part I: parametric study, Desalination, 185 (2005) 427–437.

[16] N. Guettaï, H. Ait Amar, Photocatalytic oxidation of methyl orange in presence of titanium dioxide in aqueous suspension. Part II: kinetics study, Desalination, 185 (2005) 439–448.

[17] Z. Yousefi, R.-A. Mohmadpour, E. Zarei, M. Barafrashtehpour, Lignin degradation from synthetic wastewater of pulp and paper industries by using of UV/Fe-doped TiO_2 photocatalytic process, J. Mazandaran Univ. Med. Sci., 23 (2014) 96–106.

[18] T. Kaur, A. Sraw, R.K. Wanchoo, A.P. Toor, Visible–light induced photocatalytic degradation of fungicide with Fe and Si doped TiO_2 nanoparticles, Mater. Today:. Proc., 3 (2016) 354–361.

[19] X. Cheng, X. Yu, Z. Xing, Characterization and mechanism analysis of N doped TiO_2 with visible light response and its enhanced visible activity, Appl. Surf. Sci., 258 (2012) 3244–3248.

[20] A. Dargahi, A. Ansari, D. Nematollahi, G. Asgari, R. Shokoohi, M.R. Samarghandi, Parameter optimization and degradation mechanism for electrocatalytic degradation of 2, 4-dicloro-phenoxyacetic acid (2, 4-D) herbicide by lead dioxide electrodes, RSC Adv., 9 (2019) 5064–5075.

[21] Y. Abdollahi, A.H. Abdullah, Z. Zainal, N.A. Yusof, Photo-degradation of *p*-cresol by zinc oxide under visible light, Int. J. Appl. Sci. Technol., 1 (2011) 99–105.

[22] S. Moghaddam, M.M. Zerafat, S. Sabbaghi, Response surface methodology for optimization of Phenol photo-catalytic degra-dation using Carbon-doped TiO_2 nano-photocatalyst, Int. J. Nano Dimens., 9 (2018) 89–103.

[23] A. Felix, A. Amenaghawon, A. Mededode, Heterogeneous photocatalytic degradation of naphthalene using periwinkle shell ash: effect of operating variables, kinetic and isotherm study, South African J. Chem. Eng., 19 (2014) 31–45.

[24] Y. Abdollahi, A.H. Abdullah, Z. Zainal, N.A. Yusof, Photo-degradation of *m*-cresol by zinc oxide under visible-light irra-diation, Int. J. Chem., 3 (2011) 31.

[25] A. Almasi, A. Dargahi, M. Mohammadi, A. Azizi, A. Karami, F. Baniamerian, Z. Saeidimoghadam, Application of response surface methodology on cefixime removal from aqueous solution by ultrasonic/photooxidation, Int. J. Pharm. Sci. Technol., 8 (2016) 16728–16736

[26] E. Bazrafshan, S. Noorzaei, F. KordMostafapour, Photocatalytic degradation of aniline in aqueous solutions using magnesium oxide nanoparticles, J. Mazandaran Univ. Med. Sci., 26 (2016) 126–136.

[27] A. Kumar, G. Pandey, A Review on the factors affecting the photocatalytic degradation of hazardous materials, Mater. Sci. Eng. Int. J., 1 (2017) 00018.

[28] D. Rajamanickam, M. Shanthi, Photocatalytic degradation of an organic pollutant by zinc oxide – solar process, Arabian J. Chem., 9 (2016) S1858–S1868.

[29] S.M. Borghei, S.N. Hosseini, Comparison of furfural degradation by different photooxidation methods, Chem. Eng. J., 139 (2008) 482–488.

[30] A.K. Sahu, V.C. Srivastava, I.D. Mall, D.H. Lataye, Adsorption of furfural from aqueous solution onto activated carbon: kinetic, equilibrium and thermodynamic study, Sep. Sci. Technol., 43 (2008) 1239–1259.

[31] K. Chun-li, T. Xiao-jian, J. Xin-qian, G. Ping, Q. Fu-min, L. Xue-yu, Degradation of furfural by UV/O_3 technology, Chem. Res. Chinese U, 25 (2009) 451–454.

[32] M. Zhou, J. Yu, B. Cheng, Effects of Fe-doping on the photo-catalytic activity of mesoporous TiO_2 powders prepared by an ultrasonic method, J. Hazard. Mater., 137 (2006) 1838–1847.

[33] F. Veisi, M.A. Zazouli, M.A. Ebrahimzadeh, J.Y. Charati, A.S. Dezfoli, Photocatalytic degradation of furfural in aqueous solution by N-doped titanium dioxide nanoparticles, Environ. Sci. Pollut. Res., 23 (2016) 21846–21860.